A Quasi-One-Dimensional Theory for Anisotropic Propagation of Excitation in Cardiac Muscle

Jiashin Wu,*# Edward A. Johnson,* and J. Mailen Kootsey*§
*Department of Cell Biology, Duke University Medical Center, Durham, North Carolina 27710; #Department of Physics and Astronomy, Vanderbilt University, Nashville, Tennessee 37235; and §Andrews University, Berrien Springs, Michigan 49104 USA

ABSTRACT It has been shown that propagation of excitation in cardiac muscle is anisotropic. Compared to propagation at right angles to the long axes of the fibers, propagation along the long axis is faster, the extracellular action potential (AP) is larger in amplitude, and the intracellular AP has a lower maximum rate of depolarization, a larger time constant of the foot, and a lower peak amplitude. These observations are contrary to the predictions of classical one-dimensional (1-D) cable theory and, thus far, no satisfactory theory for them has been reported. As an alternative description of propagation in cardiac muscle, this study provides a quasi-1-D theory that includes a simplified description of the effects of action currents in extracellular space as well as resistive coupling between surface and deeper fibers in cardiac muscle. In terms of classical 1-D theory, this quasi-1-D theory reveals that the anisotropies in the wave form of the AP arise from modifications in the effective membrane ionic current and capacitance. The theory also shows that it is propagation in the longitudinal, not in the transverse direction that deviates from classical 1-D cable theory.

NOMENCLATURE

a	radius of the fiber (cm)
r_i	intracellular resistance per unit axial length of the fiber in the axial (x) direction (kΩ/cm)
r_e	extracellular axial resistance per unit axial length of the fiber in the axial (x) direction (kΩ/cm)
r_d	depth resistance per unit axial length of the fiber (kΩ cm)
c_m	specific membrane capacitance per unit axial length of the fiber (μF/cm)
R_i	specific intracellular resistivity of the fiber (kΩ cm)
R_i^z	intercellular coupling resistivity along the z axis (kΩ cm)
R_e	extracellular axial resistivity of the fiber (kΩ cm)
R_d	depth resistance per unit area of membrane surface of the fiber (kΩ cm^2)
C_m	specific membrane capacitance per unit area of membrane surface of the fiber (μF/cm^2)
γ	ratio of intracellular to extracellular equivalent cross section areas
$i_i(x, t)$	intracellular axial current (μA)
$i_i^z(x, t)$	intercellular exchange current per unit length of fiber at z direction for a fiber on the surface of muscle (μA/cm)
$i_e(x, t)$	extracellular axial current (μA)
$i_i^z(x, t)$	extracellular exchange current per unit length of fiber at z direction for a fiber on the surface of muscle (μA/cm)
$I_d(x, t)$	extracellular depth current per unit axial length of fiber for a fiber on the surface of muscle (μA/cm)
$I_m(x, t)$	transmembrane current per unit axial length of fiber (μA/cm)
$i_{ion}(x, t)$	transmembrane ionic current per unit axial length of fiber (μA/cm)
$I_{ion}(x, t)$	transmembrane ionic current density on the surface of fiber (μA/cm^2)
$I_i^z(x, t)$	intercellular exchange current density at z direction for a fiber on the surface of muscle (μA/cm^2)
$I_{app}(x, t)$	apparent transmembrane ionic current density on the surface of fiber (μA/cm^2)
$V_i(x, t)$	intracellular potential with reference electrode in the depth of extracellular space (mV)
$V_e(x, t)$	extracellular potential at the surface of cell membrane with reference electrode in the depth of extracellular space (mV)
$V_m(x, t)$	transmembrane potential (mV)
t	time (ms)
x	the axis representing the direction of surface propagation, which may represent either the transverse or longitudinal direction relative to the long axis of the fiber, depending on what direction of propagation is being simulated (cm)
z	the direction perpendicular to the surface plane of the muscle (cm)
θ_x	velocity of the steady propagation of $V_m(x, t)$ along the x axis (cm/ms)

Received for publication 17 April 1996 and in final form 16 August 1996.
Address reprint requests to Dr. Jiashin Wu, Department of Physics and Astronomy, Vanderbilt University, Box 1807, Station B, Nashville, TN 37235. Tel.: 615-322-6361; Fax: 615-322-4977; E-mail: jiashin@dendrite.phy.vanderbilt.edu.

0006-3495/96/11/2427/13 $2.00

θ_z	velocity of the steady propagation of $V_m(x, t)$ at the z direction (cm/ms)
λ	length constant, equal to $\sqrt{r_m/(r_i + r_e)}$
g_{Na}	membrane Na^+ channel conductivity (mS/cm^2)
$\bar{g}_{Na}$	maximum membrane Na^+ conductivity (mS/cm^2)
g_{leak}	membrane leakage channel conductivity (mS/cm^2)
E_{Na}	equilibrium potential of membrane Na^+ current (mV)
E_{leak}	equilibrium potential of membrane leakage current (mV)
V_i^{peak}	peak amplitude of intracellular potential (mV)
$\dot{V}_i$	rate of rise of intracellular potential (V/s)
$\dot{V}_i^{max}$	maximum rate of rise of intracellular potential (V/s)
V_e^{pp}	peak-to-peak value of extracellular potential (mV)
V_m^{peak}	peak amplitude of transmembrane potential (mV)
$\dot{V}_m$	rate of rise of transmembrane potential (V/s)
$\dot{V}_m^{max}$	maximum rate of rise of transmembrane potential (V/s)
I_m^{max}	maximum density of transmembrane current (μA/cm^2)
I_{Na}	membrane Na^+ current density (μA/cm^2)
I_{Na}^{max}	maximum density of membrane Na^+ current (μA/cm^2)
τ_i	time constant of the foot of intracellular potential (ms)
τ_m	time constant of the foot of transmembrane potential (ms)
Δt	time step of Crank-Nicolson partial differential equation solver (μs)
Δx	length of fiber element (μm)

INTRODUCTION

Propagation of electrical excitation in cardiac muscle has been known to be anisotropic since the work of Kukushkin et al. (1975) and Clerc (1976). Kukushkin et al. observed anisotropy in the velocity of propagation of excitation, θ, in isolated strips of atrial and ventricular muscle from dog heart. They showed that θ was greater along the longitudinal axis of the fibers than in the direction at right angles to them.

Using a series of microelectrode impalements in trabeculae from the right ventricle of calf hearts, Clerc (1976) measured θ and the intracellular and extracellular resistivities along and at right angles to the fiber orientation. He showed that θ of the action potential (AP) was much faster along than at right angles to the fiber orientation and that the differences in θ and the tissue resistivities obeyed the inverse square law of classical one-dimensional (1-D) cable theory (Hodgkin and Huxley, 1952).

Roberts et al. (1979) reported anisotropies in the amplitude and the velocity of spread of the extracellular potential in the left ventricular epicardium of dog hearts in vivo. They mapped the propagation of excitation with an extracellular electrode array of 84 electrodes, applying stimuli via an electrode at the center of the array. They found that the spread of epicardial excitation was 2.4 times faster along the long axes of the muscle fibers than in a direction at right angles to them. The amplitude of the extracellular potential was approximately 3 times greater for propagation along the fiber axes than for propagation at right angles.

In 1981 Spach et al. showed that propagation of the intracellular AP in the dog heart was anisotropic in both the atrial crista terminalis and the papillary muscle of the right ventricle, although the ratio of longitudinal to transverse velocities in the papillary muscle was lower than the ratio in the crista terminalis. By stimulating at differing sites around a single intracellular recording site, they were able to generate excitation wavefronts that propagated at various angles relative to the orientation of the muscle fibers. Compared to propagation at right angles to the long axis of the muscle fibers (transverse propagation, TP), propagation along the fiber axis (longitudinal propagation, LP) was faster and was associated with an AP having a lower maximum rate of depolarization ($\dot{V}_{max}$), a larger time constant of the foot (τ_{foot}), a lower peak amplitude (V_i^{peak}), and a lower safety factor for propagation (SF). The authors pointed out that the association of faster θ with an AP having a lower V_i^{peak}, a lower $\dot{V}_{max}$, and a larger τ_{foot} was contrary to classical 1-D cable theory, which together with its extensions to 2-D (Shiba, 1971; Shiba and Kanno, 1971) and 3-D (Tung, 1978) domains, has been widely used to describe the propagation of electrical excitation in cardiac muscle. In classical 1-D cable theory, faster propagation can be caused by either a reduction in intracellular resistance per unit length of the fiber, r_i, or an increase in the membrane ionic current associated with the depolarization phase of the AP. The theory shows, however, that a change in r_i causes no change in the wave form of the AP. On the other hand, the increase in θ caused by an increase in ionic current (e.g., an increase in the density of Na^+ channels) results in an AP with a greater $\dot{V}_{max}$, a smaller τ_{foot}, and a greater V_i^{peak} (Hodgkin and Katz, 1949; Berkinblit et al., 1970), quite contrary to the findings of Spach et al. (1981). Such classical behavior has in fact been observed (Spach et al., 1981; Dominguez and Fozzard, 1979). Spach et al. (1981) stimulated thin strands of Purkinje fibers from dog heart at a regular, constant rate and an extra stimulus was interposed after every 15th stimulus at the regular rate, such that the extra stimulus fell in the relative refractory period of the preceding regular AP. The θ of the premature AP (initiated by the extra stimulus) was varied by varying the degree of prematurity of the extra stimulus relative to the preceding regular one. In this preparation, where propagation was confined to the long axis of the strand, θ, $\dot{V}_{max}$, and τ_{foot} varied exactly according to 1-D cable theory.

In the same paper, Spach et al. (1981) went on to show that the anisotropies in propagation that they had observed in the crista terminalis and papillary muscle could not have been caused by different membrane properties, e.g., by the organization of cells into a narrow tract. Reproducibly, in the same preparation and from preparation to preparation, and irrespective of the location of the stimulating electrode, isochronal excitation maps always showed propagation away from the stimulus site to be faster along the long axes of the fibers than at right angles to them. In every case, the faster the propagation at the intracellular recording site, the lower the magnitude of $\dot{V}_{max}$ and V_i^{peak} and the larger the magnitude of τ_{foot} of the AP. In 1992 Spach et al. showed that although there were differences from cell to cell in $\dot{V}_{max}$ of APs during longitudinal and transverse propagation, the same anisotropies in propagation as observed earlier still held.

THEORETICAL

That directional changes in intracellular resistance produce directional changes in θ was first shown by Joyner et al. (1975). They simulated the propagation of electrical activity in a two-dimensional representation of the thin-walled atrium and investigated the effects of anisotropy in membrane properties and intracellular resistivity on the wavefronts of propagation of electrical activity. They showed that different internal resistance in the x and y directions resulted in inhomogeneities in θ, as observed later experimentally by Clerc (1976).

It was recognized by Spach et al. (1981) that because of the anisotropy in the AP wave form as well as in θ, additional factors must be involved. They suggested that propagation might be discontinuous in the transverse direction. They based this idea on the fact that cardiac muscle fibers are arranged into long bundles of small diameter (<500 μm) (Sommer and Scherer, 1985). Within these bundles the individual fibers are electrically connected to one another through nexuses, to such a degree that the bundle effectively acts as a single fiber (Sommer and Johnson, 1979). On the other hand, such bundles are interconnected less extensively laterally, so that propagation might well be discontinuous in a direction transverse to the long axes of the bundles.

There have been several simulations of discontinuous propagation in cardiac muscle. Diaz et al. (1982) built a 1-D model, with excitable cells described by the Beeler-Reuter model for ventricular muscle (Beeler and Reuter, 1977), in which the kinetics of the excitatory Na^+ current are described by empirically modified Hodgkin-Huxley equations (Hodgkin and Huxley, 1952). Individual cells were separated by resistive intercalated discs. They showed that this model could account for the anisotropies in θ and in $\dot{V}_{max}$, but the model failed to account for the anisotropy in τ_{foot}. In their simulations the more slowly propagating APs had a larger rather than a smaller τ_{foot}. Similar results were reported by Joyner (1982), Spach and Kootsey (1983), Rudy and Quan (1987), and Leon and Roberge (1991).

Using a two-dimensional (2-D), bidomain (intra- and extracellular spaces) model of cardiac muscle, Kootsey and Wu (1991) showed that an anisotropic action potential could be generated if the extracellular space had resistive elements along the depth of extracellular space as well as along the membrane surface. When they reduced the resistivity of the extracellular space to zero, the anisotropy in the wave form of AP was eliminated. With a 2-D bidomain model representing a cross section of a block of cardiac muscle in bath, Pollard et al. (1992) explored the effects of anisotropies in tissue resistivities. Similar to the work by Kootsey and Wu, the results of Pollard et al. also suggest that the influence of the extracellular volume conductor might be one factor causing the anisotropies in propagation observed by Spach et al. (1981). However, the size of the spatial discreteness in the simulation by Pollard et al. was too big, 32 μm for both along and transverse to the fibers. As discussed later in this paragraph, this size would likely introduce digitization errors in the wave form of the AP, especially for the transverse direction, which had high equivalent intracellular resistivity for the bidomain model they used. The same discretization problem also occurred in the simulation of a block of cardiac tissue in a bathing solution made by Henriquez and Papazoglou (1993). Using the Ebihara-Johnson (Ebihara and Johnson, 1980) membrane, they demonstrated that anisotropic phase plots of APs could be generated in a bidomain block with unequal anisotropic ratios of resistivities in contact with a volume conductor. However, they did not show any of the other anisotropies observed in the experiments of Spach et al. (1979, 1981, 1987). Furthermore, the spatial discretizations they used along the fibers, Δx, at right angles to the fibers, Δy, and into the tissue, Δz, were 40 μm, 25 μm, and 40 μm, respectively. Spach and Kootsey (1983) simulated discontinuous propagation by changing the value of spatial discretization Δx in the numerical solution of the classical 1-D cable equation. Using a cable model with the Na^+ current described by Ebihara-Johnson equations, they computed θ and the wave form of the AP for different values of axial resistivity in a simulated elongated cell 10 μm in diameter. At low values of Δx (5 and 10 μm), θ and the shape of the AP were indistinguishable from that for a continuous cable. When Δx was increased to 40 μm, θ deviated less than 7.8% from that for a continuous cable. However, τ_{foot} increased 23% and $\dot{V}_{max}$ increased 34%, showing that discretization could cause large changes in the shape of the AP, whereas θ was changed only slightly. The overall effects of discretization on the wave form of the AP were inconsistent with the observed anisotropies: τ_{foot} increased rather than decreased as θ decreased. Spach et al. (1987) simulated propagation of the AP along a 1-D fiber for different specific membrane capacitance and compared the simulation results to their experimental observations. They showed that a difference in specific membrane capacitance in the two directions of propagation (combined with directional differences in effective axial resistivity) could account for all of the characteristics of anisotropic propagation. However, they could

provide no explanation of how such a difference in membrane capacitance could occur.

In the present study we develop a quasi-1-D cable theory that adds two components of current flow to the classical 1-D cable theory: 1) a first approximation to 2-D current flow in extracellular space and 2) the exchange of excitatory current between superficial and deeper fibers. Together with the known anisotropy in resistivities of cardiac muscle, simulations with this quasi-1-D model produce anisotropies in propagation similar to those observed by Spach et al. (1981). Furthermore, we show that the effects of current exchange between fibers on the propagation of activation are equivalent to those generated by directional differences in the effective membrane capacitance as hypothesized by Spach et al. (1987), thereby providing a rational basis for their hypothesis.

The second part of this study presents a simulation model for the same phenomena of anisotropic propagation. For the purpose of verifying the quasi-1-D theory, the simulation model was developed separately without using the quasi-1-D equations, although both the quasi-1-D theory and the simulation are targeted to the same anisotropic propagation and the same tissue structure. Their differences are in the level of abstraction and in the technical approaches. We did not use any curve fit in this study. Instead, both the theory and the simulation are based on the experimental observations and on the experimentally measured parameters.

DERIVATION OF A QUASI-1-D CABLE THEORY FOR PROPAGATION IN CARDIAC MUSCLE

Although cardiac muscle is three dimensional, the wave fronts of longitudinal and transverse anisotropic propagations approach plane wave fronts when sufficiently far away from the stimulation site, as shown in the experiments of Spach et al. (1981). Propagation therefore becomes essentially 1-D in each direction. As a consequence, we can study anisotropic propagation in the two directions separately, along and at right angles to the fibers.

$$\frac{a}{2(R_i + \gamma R_e)\theta^2}\frac{\partial^2 V_m(x, t)}{\partial t^2} = C_m\frac{\partial V_m(x, t)}{\partial t} + I_{ion}(x, t). \quad (1)$$

Equation 1 is the classical 1-D cable equation when steady propagation is established. As shown by Hodgkin and Katz (1949), the waveform of the AP is only affected by local membrane properties, i.e., the capacitance and ionic current of membrane, but not by the tissue resistivity. The right-hand side of Eq. 1 is solely dependent on the local membrane properties and is independent of spatial properties. If local membrane properties do not change, $(R_i + \gamma R_e)\theta^2$ is constant. Any change in axial resistivity only results in a change in θ; the waveform of AP remains unchanged.

A fundamental assumption of classical 1-D cable theory is that the action currents associated with the propagation of excitation flow in one direction only, namely along the long axis of the fiber. For a long cylindrical or ribbon-shaped cell, in which one dimension exceeds all others, and provided that the length constant, λ, during excitation does not approach any of the smaller dimensions, such as the diameter of the cylinder or the width of the ribbon, this assumption is reasonable for intracellular current flow. For current flow in extracellular space this is rarely a reasonable assumption. An exception, mentioned previously, is that of a single, long, isolated muscle or nerve in oil, where the conductive pathway in extracellular space is reduced to a thin surface film (Hodgkin and Rushton, 1946). In most other experimental situations, the potential variations in extracellular space are assumed to be negligibly small, as indeed they are in many circumstances, e.g., single isolated skeletal muscle and nerve fibers.

However, in the case of a multicellular tissue such as cardiac muscle, this often is not the case. The action currents of fibers in the deeper regions of the tissue produce significant changes in extracellular potential and hence in transmembrane potential. Furthermore, current flow occurs between surface and deeper fibers through intercellular nexuses. Perhaps these factors are responsible, at least in part, for the observed anisotropies in propagation. With this in mind, we derive a quasi-1-D cable theory that includes a simplified description of current flow in extracellular space and current coupling between the surface and deeper fibers.

We will assume, as a first approximation, that a cardiac muscle fiber is a continuous 1-D structure composed of a conductive, capacitive membrane separating purely conductive intracellular and extracellular spaces. This fiber is at the surface of a piece of muscle immersed in a bathing solution, and is coupled, intracellularly, to adjacent fibers beneath via resistive connections. That is to say, there is an intercellular resistivity, R_i^z, connecting the intracellular spaces of adjacent fibers in the z direction, perpendicular to the surface plane of the muscle. The intracellular current consists of two components: one travels along the long axis of the fiber, $i_i(x, t)$, as in classical 1-D theory; the other intracellular component of current, $i_i^z(x, t)$, exchange current, flows into deeper fibers in a direction perpendicular to the surface of the muscle through resistive intercellular connections. In the quasi-1-D equations that we are going to present, the intracellular exchange current is only defined on the fiber, although its direction is perpendicular to the fiber. Therefore, it acts like a current source/sink to the intracellular domain of the 1-D fiber. When we consider propagation along the long axis of the fibers, $i_i(x, t)$ will represent current flowing intracellularly in that direction; when we consider propagation in a direction at right angles to the long axis of the fibers, $i_i(x, t)$ will represent the current flowing intracellularly in that direction, i.e., at right angles to the fibers.

In general, extracellular space behaves as a volume conductor and as such is usually described by volume conductor theory. However, in the present circumstance it is useful to approximate the effect of current flow in such a conductor by assuming that current can flow in two directions, 1) longitudinally along the membrane surface as in 1-D theory ($i_e(x, t)$), and 2) away from the membrane surface into

extracellular space. Similar to the intracellular domain, the second component of the extracellular current flowing away from the membrane surface is also only defined on the surface of the membrane along the fiber. This current is the source/sink of the extracellular axial current along the fiber. The extracellular sink/source current can be different from the intracellular exchange (source/sink) current. Therefore, it can be further break down to two components: 1) an exchange current, $i_e^z(x, t)$, representing the returning current associated with the intracellular exchange current, $i_i^z(x, t)$, and 2) current flowing into the depths of the tissue, $i_d(x, t)$. Because $i_i^z(x, t)$ and $i_e^z(x, t)$ form a current loop, $i_d(x, t)$ is the net current flowing from the fiber to the remote ground in the bath. Because all currents are defined along the fiber, although they have different directions, we ignored the complexity of the space distribution of the extracellular depth current. The ratio of extracellular surface potential (V_e) to the extracellular depth current $i_d(x, t)$ is represented by the depth resistance R_d. Thus extracellular space has an axial (fiber surface) resistivity, R_e, a depth resistivity, R_d, and an interstitial resistivity, R_e^z, for $i_e(x, t)$, $i_d(x, t)$, and, $i_e^z(x, t)$, respectively. Although the directions of $i_i^z(x, t)$, $i_e^z(x, t)$, and $i_d(x, t)$ are perpendicular to the fiber, they are all defined on the fiber, i.e., in quasi-one-dimension. In summary, the quasi-1-D theory describes a 1-D fiber with current sinks/sources at both intracellular and extracellular spaces. The current sinks/sources represent the interactions of the surface fiber with the fibers beneath it in the tissue and with the bath above it.

The addition of an extracellular depth current, $i_d(x, t)$, provides a first approximation to a volume conductor and, as will be shown later, gives rise to biphasic extracellular potentials during propagation similar to those recorded experimentally. Because this study is concerned primarily with anisotropic propagation in isolated preparations of cardiac muscle of relatively simple structure and not with the actual spatial distribution of extracellular current, this simplified representation of extracellular resistivities is reasonable and greatly simplifies the numerical computation.

These current pathways are illustrated diagrammatically in Fig. 1.

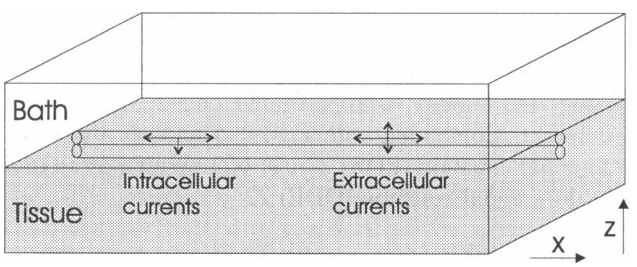

FIGURE 1 The quasi 1-D theory describes the propagation of activation along the x direction on the surface of a tissue block in a bath. A surface fiber has connections with adjacent fibers. z is the direction perpendicular to the surface plane of the tissue.

Relevant equations

Equations 2–6 are the relevant equations relating r_i, r_e, r_d, c_m, and $i_{ion}(x, t)$ to their corresponding specific counterparts, R_i, R_e, R_d, C_m, and $I_{ion}(x, t)$.

The intracellular resistance per unit length of the fiber, r_i, is given by

$$r_i = \frac{R_i}{\pi a^2}, \tag{2}$$

where R_i is the resistivity of intracellular space, a is the radius of the fiber, and π has its usual meaning. Similarly, the extracellular resistance per unit length of the fiber, r_e, is given by

$$r_e = \frac{\gamma R_e}{\pi a^2}, \tag{3}$$

where R_e is the resistivity of bulk extracellular space, and γ is the ratio of the equivalent cross-sectional areas of intracellular and extracellular space.

The unit resistance to extracellular current flow into the depths of the tissue, perpendicular to the surface of the fiber, is defined in terms of the fiber length, i.e., as a depth resistance per unit length of the fiber, r_d, given by

$$r_d = \frac{R_d}{2\pi a}, \tag{4}$$

where R_d is the depth resistance per unit area of membrane.

The membrane capacitance per unit length of the fiber, c_m, is given by

$$c_m = 2\pi a C_m. \tag{5}$$

where C_m is the specific membrane capacitance.

The ionic current per unit length of the fiber, $i_{ion}(x, t)$, is given by

$$i_{ion}(x, t) = 2\pi a I_{ion}(x, t), \tag{6}$$

where $I_{ion}(x, t)$ is the ionic current per unit area of membrane.

The transmembrane potential, $V_m(x, t)$, inside with respect to a point immediately outside the fiber, is given by

$$V_m(x, t) = V_i(x, t) - V_e(x, t), \tag{7}$$

$V_i(x, t)$ is the intracellular potential and $V_e(x, t)$ is the extracellular potential, both with respect to a distant point outside the fiber at zero potential.

The velocity of propagation of an AP along the axis x, θ_x, is given by

$$\theta_x = \frac{dx}{dt}, \tag{8}$$

and perpendicular to the muscle surface, along axis z, θ_z, by

$$\theta_z = \frac{dz}{dt} \tag{9}$$

where t is time. θ_z is only defined at the surface of the muscle fiber.

Derivation of the quasi-1-D cable equations

For a thin sheet of parallel-aligned cardiac muscle fibers, propagation of a uniform plane wave front of excitation along or at right angles to the long axis of the fibers can be completely described by classical 1-D cable theory: all excitatory current can be assumed to be traveling intracellularly in one direction only, namely the direction of propagation, x, if the resistance of the extracellular space (bath) is low, so the potential changes in extracellular space caused by current flow there are negligibly small and extracellular space can be assumed to be isopotential. For a thick sheet of similarly aligned fibers, however, there are additional currents into the thickness of the sheet and into the extracellular space, namely in the z direction, and these currents cause significant potential differences. The currents include an intracellular exchange (intercellular) current between the surface and the deeper fibers, $i_i^z(x, t)$, together with its corresponding extracellular component (interstitial) current, $i_e^z(x, t)$, as well as an extracellular depth current, $i_d(x, t)$, leaving the fiber in the z direction, representing current spread through extracellular space. As we mentioned earlier, the currents in the z direction are only defined at the surface fibers. They act as the current source/sink to the surface fibers.

The axial voltage gradients and currents, including the extracellular depth current, obey Ohm's law, as shown in Eqs. 10–12:

$$\frac{\partial V_i(x, t)}{\partial x} = -i_i(x, t)r_i \tag{10}$$

$$\frac{\partial V_e(x, t)}{\partial x} = -i_e(x, t)r_e \tag{11}$$

$$i_d(x, t) = \frac{V_e(x, t)}{r_d}, \tag{12}$$

where $i_i(x, t)$ and $i_e(x, t)$ are the intracellular and extracellular axial currents, respectively.

The change in intracellular axial current equals the sum of the transmembrane current and i_i^z:

$$\frac{\partial i_i(x, t)}{\partial x} = -i_m(x, t) - i_i^z(x, t). \tag{13}$$

The change in extracellular axial current equals the sum of the transmembrane current $i_m(x, t)$, the $i_e^z(x, t)$, and the extracellular depth current $i_d(x, t)$:

$$\frac{\partial i_e(x, t)}{\partial x} = i_m(x, t) - i_e^z(x, t) - i_d(x, t). \tag{14}$$

The sum of intracellular and extracellular exchange currents between fibers is zero:

$$i_i^z(x, t) + i_e^z(x, t) = 0. \tag{15}$$

Equation 16 relates intercellular exchange current per unit fiber length, $i_i^z(x, t)$, to intercellular exchange current per unit area in the z direction, $I_i^z(x, t)$:

$$i_i^z(x, t) = 2aI_i^z(x, t). \tag{16}$$

Differentiating Eq. 7 yields

$$\frac{\partial V_m(x, t)}{\partial x} = \frac{\partial V_i(x, t)}{\partial x} - \frac{\partial V_e(x, t)}{\partial x}. \tag{17}$$

Substituting Eqs. 10 and 11 into Eq. 17 yields

$$\frac{\partial V_m(x, t)}{\partial x} = -r_i i_i(x, t) + r_e i_e(x, t). \tag{18}$$

Differentiating Eq. 18 again and substituting Eqs. 13 and 14 into it yields

$$\frac{\partial^2 V_m(x, t)}{\partial x^2} = (r_i + r_e)i_m(x, t) + r_i i_i^z(x, t) - r_e i_e^z(x, t) - r_e i_d(x, t). \tag{19}$$

Using Eq. 15, Eq. 19 can be rewritten as

$$\frac{\partial^2 V_m(x, t)}{\partial x^2} = (r_i + r_e)(i_m(x, t) + i_i^z(x, t)) - r_e i_d(x, t). \tag{20}$$

The transmembrane current, i_m, is the sum of membrane capacitive current and membrane ionic currents i_{ion}, i.e.,

$$i_m(x, t) = c_m\frac{\partial V_m(x, t)}{\partial t} + i_{ion}(x, t). \tag{21}$$

Putting Eqs. 12, 20, and 21 together yields

$$\frac{1}{r_i + r_e}\frac{\partial^2 V_m(x, t)}{\partial x^2} = c_m\frac{\partial V_m(x, t)}{\partial t} + i_{ion}(x, t) + i_i^z(x, t) - \frac{r_e}{r_d(r_i + r_e)}V_e(x, t). \tag{22}$$

When steady propagation of an AP is established along the fiber, the velocity of propagation along the fiber axis, θ_x, is constant. Combining with Eqs. 2–5 and 16, the partial differential equation (PDE) 22 can be rewritten as an ordinary differential equation (ODE) 23:

$$\frac{a}{2(R_i + \gamma R_e)\theta_x^2}\frac{d^2V_m(x, t)}{dt^2} = C_m\frac{dV_m(x, t)}{dt} + I_{ion}(x, t) + \frac{1}{\pi}I_i^z(x, t) - \frac{\gamma R_e}{R_d(R_i + \gamma R_e)}V_e(x, t). \tag{23}$$

The intercellular exchange current per unit surface area, $I_i^z(x, t)$, is caused by the voltage gradient in the intracellular space along direction z (perpendicular to the fiber into the depth of the muscle) and the intercellular resistivity R_i^z. During steady propagation on the surface of the muscle, the voltage gradient can be described as

$$\frac{1}{\theta_z}\frac{dV_i(x, t)}{dt}.$$

Again, both R_i^z and θ_z are defined at the surface of the fiber. They represent the properties of the current source/sink to the 1-D fiber. Therefore, Eq. 24 is obtained from Eq. 7. Here, θ_z is a constant for steady propagation on the surface of the muscle.

$$I_i^z(x, t) = \frac{1}{R_i^z\theta_z}\frac{dV_i(x, t)}{dt} = \frac{1}{R_i^z\theta_z}\left(\frac{dV_m(x, t)}{dt} + \frac{dV_e(x, t)}{dt}\right). \tag{24}$$

Substituting Eq. 24 into Eq. 23 yields

$$\frac{a}{2(R_i + \gamma R_e)\theta_x^2}\frac{d^2V_m(x, t)}{dt^2} = \left(C_m + \frac{1}{\pi R_i^z\theta_z}\right)\frac{dV_m(x, t)}{dt} \tag{25}$$

$$+ I_{ion}(x, t) - \frac{\gamma R_e}{R_d(R_i + \gamma R_e)}V_e(x, t) + \frac{1}{\pi R_i^z\theta_z}\frac{dV_e(x, t)}{dt}.$$

Here we define an apparent membrane capacitance C_{app}, given by

$$C_{app} = C_m + \frac{1}{\pi R_i^z\theta_z}, \tag{26}$$

and an apparent membrane ionic current I_{app}, given by

$$I_{app}(x, t) = I_{ion}(x, t) - \frac{\gamma R_e}{R_d(R_i + \gamma R_e)}V_e(x, t) + \frac{1}{\pi R_i^z\theta_z}\frac{dV_e(x, t)}{dt}. \tag{27}$$

Then Eq. 25 can be rewritten to give

$$\frac{a}{2(R_i + \gamma R_e)\theta_x^2}\frac{d^2V_m(x, t)}{dt^2} = C_{app}\frac{dV_m(x, t)}{dt} + I_{app}(x, t). \tag{28}$$

Equation 28 is similar to the classical 1-D cable equation, except that both the membrane capacitance and transmembrane ionic current are replaced by the apparent membrane capacitance and the apparent membrane ionic current. In the rest of the paper, the difference between C_{app} and C_m, $1/\pi R_i^z\theta_z$, will be referred to as the virtual membrane capacitance. Furthermore, the difference between $I_{app}(x, t)$ and I_{ion},

$$-\frac{\gamma R_e}{R_e(R_i + \gamma R_e)}V_e(x, t) + \frac{1}{\pi R_i^z\theta_z}\frac{dV_e(x, t)}{dt},$$

will be referred as the virtual membrane ionic current.

Differentiating Eq. 11 and combining the result with Eq. 14 yields

$$\frac{\partial^2V_e(x, t)}{\partial x^2} = -\frac{\partial i_e(x, t)}{\partial x}r_e = (i_d(x, t) - i_m(x, t) + i_e^z(x, t))r_e. \tag{29}$$

Rearranging Eq. 29 yields

$$i_m(x, t) = i_d(x, t) + i_e^z(x, t) - \frac{1}{r_e}\frac{\partial^2V_e(x, t)}{\partial x^2}. \tag{30}$$

Substituting Eqs. 12, 15, and 30 into Eq. 20, and then moving $V_e(x, t)$ to the left of the equation yields

$$\frac{r_i}{r_d}V_e(x, t) = \frac{\partial^2V_m(x, t)}{\partial x^2} + \left(1 + \frac{r_i}{r_e}\right)\frac{\partial^2V_e(x, t)}{\partial x^2}. \tag{31}$$

Because r_i is not zero in the tissue, Eq. 31 can be rewritten as Eq. 32:

$$\frac{1}{r_d}V_e(x, t) = \frac{1}{r_i}\frac{\partial^2V_m(x, t)}{\partial x^2} + \left(\frac{1}{r_i} + \frac{1}{r_e}\right)\frac{\partial^2V_e(x, t)}{\partial x^2}. \tag{32}$$

Putting Eqs. 2–4 and 8 into Eq. 32 and rearranging yields

$$\frac{2\theta_x^2}{aR_d}V_e(x, t) - \left(\frac{1}{R_i} + \frac{1}{\gamma R_e}\right)\frac{\partial^2V_e(x, t)}{\partial t^2} = \frac{1}{R_i}\frac{\partial^2V_m(x, t)}{\partial t^2}. \tag{33}$$

Equation 33 does not contain $i_i^z(x, t)$ or $i_e^z(x, t)$. Therefore, $i_i^z(x, t)$ and $i_e^z(x, t)$ are not involved in the extracellular potential, but form a closed local current loop perpendicular to the fiber axis. Equations 32 and 33 show the relationship among $V_e(x, t)$, $\partial^2V_m(x, t)/\partial t^2$, and $\partial^2V_e(x, t)/\partial t^2$. Depending on the tissue resistivity, the waveform of the extracellular potential may approach $V_m(x, t)$ or $\partial^2V_m(x, t)/\partial t^2$, as shown by the general theory for a 1-D fiber in a volume conductor (Plonsey, 1974).

Differentiating Eq. 10 and then combining with Eq. 13 yields

$$\frac{\partial^2V_i(x, t)}{\partial x^2} = r_i i_m(x, t) + r_i i_i^z(x, t). \tag{34}$$

Differentiating Eq. 7 twice and substituting the resulting equation with Eqs. 12, 15, 29, and 34 yields Eqs. 35 and 36:

$$\frac{\partial^2V_m(x, t)}{\partial x^2} = \left(1 + \frac{r_e}{r_i}\right)\frac{\partial^2V_i(x, t)}{\partial x^2} - \frac{r_e}{r_d}V_e(x, t) \tag{35}$$

$$\frac{\partial^2V_e(x, t)}{\partial x^2} = -\frac{r_e}{r_i}\frac{\partial^2V_i(x, t)}{\partial x^2} + \frac{r_e}{r_d}V_e(x, t). \tag{36}$$

Equation 35 shows the relationship between $V_m(x, t)$ and $V_i(x, t)$. When the magnitude of $V_e(x, t)$ becomes significant, $V_i(x, t)$ is no longer linearly related to $V_m(x, t)$. When R_d is very large, the effects of the spatial spread of current in extracellular space are minimized so that $V_i(x, t)$ becomes linearly related to $V_m(x, t)$. Equation 36 shows the corresponding relationship between $V_i(x, t)$ and $V_e(x, t)$. $i_i^z(x, t)$

and $i_e^z(x, t)$ do not affect the relative relationships among $V_i(x, t)$, $V_m(x, t)$, and $V_e(x, t)$.

SIMULATION

Morphological considerations

The shape of most ventricular working myocytes of mammalian heart approximates a long cylinder with a length of about 30–130 μm and a width of about 8–20 μm (Sommer and Scherer, 1985). The nexuses, located at or close to the ends of these long cylindrical cells, form side-to-side electrical connections between adjacent cells. Cardiac cells are linked to each other both side to side and end to end to form bundles. Johnson and Sommer (1967) examined the structure of a small bundle of rabbit heart muscle (~60 μm O.D.) containing about 13 fibers (in any given cross section) with light and electron microscopy. They evaluated the extent and distribution of regions of close cell apposition in a ~140-μm length of the strand with 1-μm-thick serial cross sections and demonstrated the distribution of possible regions of resistive coupling between fibers. They found that the lateral connections between fibers were very frequent, in that all fibers within the strand were connected laterally with one another within the 140-μm length examined. They concluded that the frequency of connections was such that were a single fiber to be excited at any point in the strand, excitation would spread to all fibers in the strand and a uniform wave front would be established within ~100 μm from the point of excitation. Hoyt et al. (1989) showed that individual myocytes were connected at intercalated disks to an average of 9.1 other myocytes in canine left ventricle.

The elongated shape of myocyte generates the anisotropic resistivity in the intracellular space. Let us assume that the intracellular resistivity is mostly concentrated at the nexus by assigning r_n as the resistance of the nexus between two neighboring myocytes and k as the geometrical ratio of the length to width of the myocytes. For a square array of myocytes arranged side by side in parallel, with the length of the side equal to the length of a myocyte, there is one myocyte along the length of myocytes, and k myocytes in the transverse direction (TD). In the longitudinal direction (LD) in the square, k myocytes are in parallel. Thus the LD resistance is r_n/k. Along the TD in the square, there are k myocytes in series. Thus the TD resistance is kr_n. Therefore, the anisotropic ratio of resistance of TD versus LD is k^2, and so transverse resistivity is much higher than longitudinal resistivity.

The anisotropic ratio of extracellular resistivity, however, is much lower than that for intracellular space (k^2). Except where cells form intercalated disks, the cells of working cardiac muscle of mammals are widely spaced, separated by 1 μm or more of contiguous extracellular space (Sommer and Johnson, 1979; Sommer and Scherer, 1985). As a consequence, current flow in extracellular space is much less restricted than that in intracellular space.

The simulation model and its parameters

Both the intracellular and the extracellular current sources/sinks are new to the theory. At this moment, there are no published experimental measurements for θ_z and R_d. (The experiment must be designed with quasi-1-D equations in mind.) Therefore, we could not translate the quasi-1-D equations directly into a simulation model without introducing arbitrary parameters. To be as faithful to the cardiac muscle as possible, we used only the experimentally measured parameters in our simulation models. Without the measured R_d and θ_z, we could not abstract the bath and the muscle fibers beneath the surface. Therefore we described them in detail in the model. The simulation model presented here is a vertical section of the cardiac muscle in bath. Although the simulation is not a direct translation of the quasi-1-D equations, both are representations of the same tissue in bath. The difference is in the degree of abstraction. They are two different and complementary approaches to the same problem. Because both the quasi-1-D theory and the model used similar structures, but the development of the equations and simulations were separate, the equations of the quasi-1-D theory and the results of the simulations could verify and complement each other. The θ_z and R_d can be used in the future after they are measured.

The simulation model was based on the equivalent structure of the circuit diagram shown in Fig. 2. Because of the long spatial interval between the recording and the stimu-

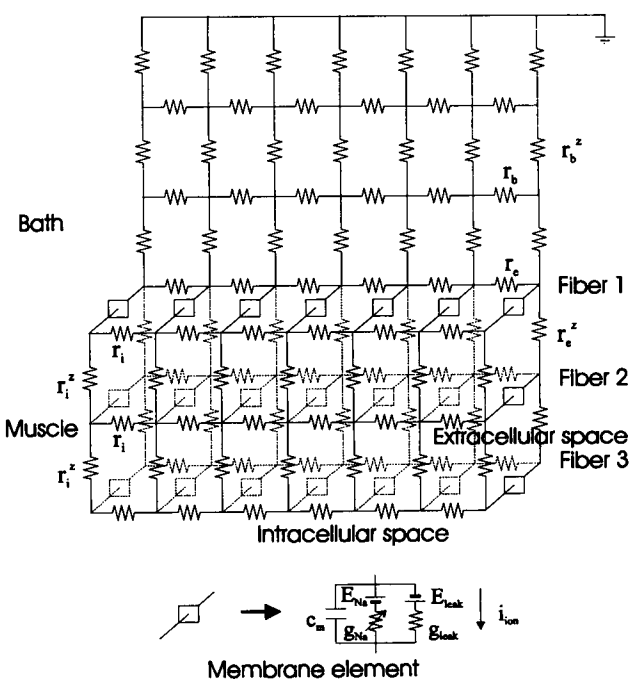

FIGURE 2 A simplified representation of the model of a vertical cross section of a block of muscle in a bath. r_i, r_e, and r_b, intracellular, extracellular, and bath longitudinal resistors. r_i^z, r_e^z, and r_b^z, intracellular, extracellular, and bath transverse resistors. c_m, membrane capacitance. i_{ion}, membrane ionic current. g_{Na}, g_{leak}, E_{Na}, and E_{leak} are the sodium and leak conductances, and the sodium and leak equilibrium potentials, respectively.

lation sites, the wave front of activation in the experiment by Spach et al. (1981) was relatively flat, with very little lateral current. Therefore, the plane wave front propagation in a 3-D block can be simplified to the propagation in a 2-D vertical cross section with its surface parallel to the direction of propagation.

A vertical cross section of a block of cardiac muscle in bath is represented by a model that consists of 40 interconnected parallel cell fibers and 100 rows of the bath elements. Each cell fiber has a 10-μm diameter and contains 200 to 300 10-μm-long elements. The fibers are arranged in a side-to-side fashion from the surface to the depth of the tissue, giving a tissue depth of 0.4 mm and a length of 2–3 mm. The bath elements are rectangular in shape, with the same length as a cell element and the same width as the cell diameter. Each row of the bath contains the same number of elements as each tissue fiber. The first and last rows of the bath elements are in contact with the top fiber in the muscle and with the ground, respectively.

Along the muscle fibers, intracellular and extracellular spaces are represented by series of interconnected resistors, r_i and r_e. There are also lateral connections between fibers, represented by intracellular transverse resistors, r_i^z, connecting each neighboring pairs of intracellular nodes from two adjacent fibers. In addition, extracellular transverse resistors, r_e^z, connect each neighboring pair of extracellular nodes at right angles to the fiber. The bath elements are connected longitudinally and transversely by r_b and r_b^z. Leakage and Na^+ current paths across the membrane link intracellular and extracellular spaces. Details of the membrane element represented by the box are shown in the insert in Fig. 2: g_{Na} and g_{leak}, and E_{Na} and E_K are the sodium and leak conductances, and the sodium and potassium equilibrium potentials, respectively. c_m is the membrane capacitance.

The values of most of the passive parameters, as well as the kinetics of the Na^+ current used, originated from the experiments on embryonic chick heart cells grown in tissue culture. The Ebihara-Johnson kinetics (Ebihara and Johnson, 1980) was used for the transmembrane Na^+ current. The Ebihara-Johnson description of the Na^+ current in cardiac muscle is still the only published experimental measurement of cardiac Na^+ current with a normal extracellular Na^+ concentration at normal temperature. The specific membrane capacitance C_m was 1.3 μF/cm^2, as measured experimentally on spherical clusters of embryonic chick heart cell by Mathias et al. (1981). The maximum membrane Na^+ conductivity of 23 mS/cm^2 was taken from Ebihara and Johnson (1980) for spherical clusters of chick heart cells. The membrane leakage conductivity, g_{leak}, was 0.05 mS/cm^2, being the specific resting membrane conductance of synthetic strands of chick cardiac muscle, as measured by Lieberman et al. (1975). The Na^+ equilibrium potential E_{Na} was 40 mV and the K^+ equilibrium potential E_K was -75 mV.

Both specific intracellular and extracellular axial resistivities were 180 Ω cm, as measured in a synthetic strand of chick cardiac muscle by Lieberman et al. (1975). This value gave a θ of 0.46 m/s, similar to the 0.5 m/s observed experimentally for longitudinal propagation in a papillary muscle of the ventricle of dog by Spach et al. (1981). Although the resistivity of interstitial space was ~51 Ω cm, its cross-sectional area was smaller compared to that of intracellular space in the ratio of ~1:3; therefore, the effective longitudinal resistance of extracellular space was ~153 Ω cm, comparable to that of intracellular space. These above default values were used unless a particular simulation was designed to evaluate the effects of altering one of them. In that case, the parameter being varied in the simulation was clearly stated in the text.

METHODS

The simulation model was written in C language. The Crank-Nicolson partial differential equation solver was used with a time step Δt of 0.5 μs to solve the propagation equations in each fiber. Each of the simulation runs required ~2 h of CPU time on a SUN Sparc 10.

R_i was changed from 180 to 18,000 Ω cm (default = 180 Ω cm) in 10 steps, covering the range of resistivity from LP to TP. Because R_i has a major effect on θ, the total number of elements and Δx had to be changed appropriately to maintain the accuracy of the computation. For higher R_i, Δx was reduced in three steps from 10 μm to 2.5 μm. A stimulus, 0.5 ms in duration and 0.02 μA in amplitude, was applied to the first intracellular elements of each fiber at the starting time.

All data in the figures were obtained from the middle point of the surface fiber to minimize the boundary and stimulus artifacts. The evaluation of these artifacts, which are negligible for the results sampled at the middle of the fiber, is shown in the Results.

Simulation results

As can be seen, the behavior of the simulated intracellular potential of the model closely resembles the experimental observations of Spach (1983). The top panels of Fig. 3 (*a–d*) show the simulation results corresponding to the experimental findings of Spach et al. (1981), shown in the bottom panels of Fig. 3 (*e–h*).

Fig. 4 shows how θ, the peak amplitudes (V_i^{peak} and V_m^{peak}), the maximum rates of depolarization ($\dot{V}_i^{max}$ and V_m^{max}) and the time constants of the foot of the intracellular and transmembrane potentials (τ_i and τ_m) vary with the intracellular resistivity (R_i). In general, high R_i (TP) is associated with low values of θ (Fig. 4 *a*), τ_i, and τ_m, (Fig. 4 *d*), as well as small extracellular APs (cf. V_e in Fig. 3 *c*), together with high values of V_i^{peak}, V_m^{peak} (Fig. 4 *b*) and $\dot{V}_i^{max}$, $\dot{V}_m^{max}$ (Fig. 4 *c*). On the other hand, low R_i (LP) is associated with high values of θ (Fig. 4 *a*), τ_i, τ_m (Fig. 4 *d*), and V_e (cf. Fig. 3 *c*), but with low values of V_i^{peak}, V_m^{peak} (Fig. 4 *b*) and $\dot{V}_i^{max}$, $\dot{V}_m^{max}$ (Fig. 4 *c*). Fig. 5 shows how the time difference of activation between the surface and the

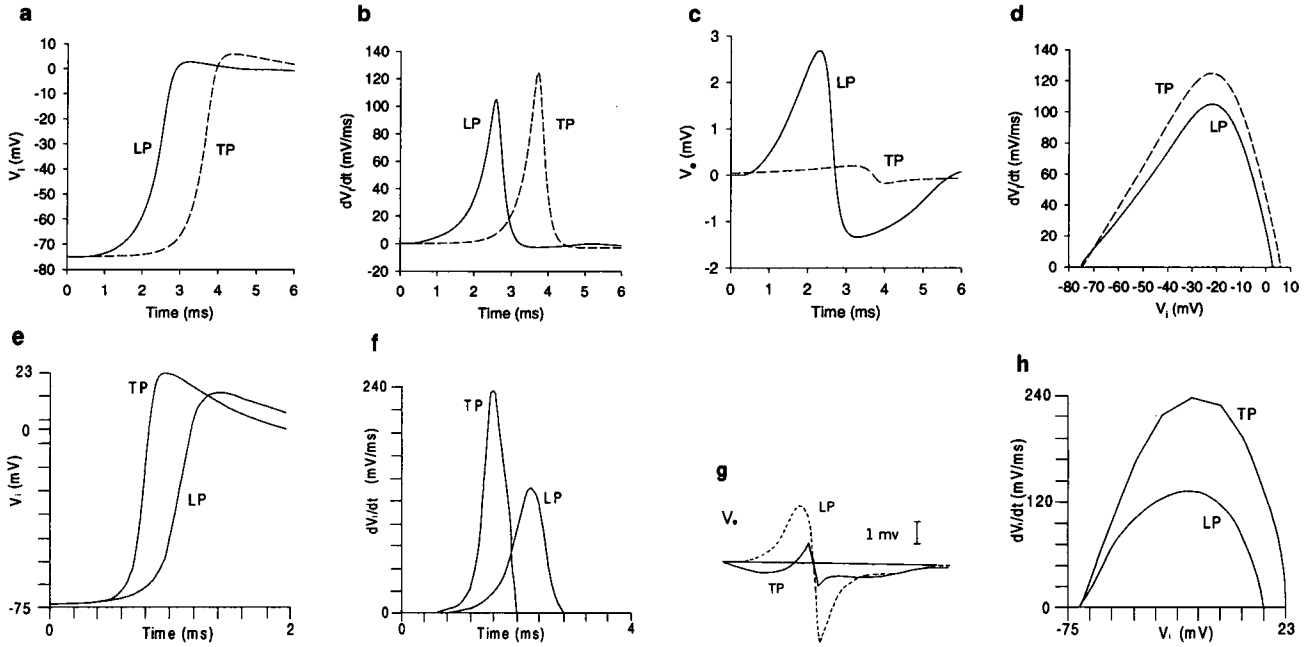

FIGURE 3 Comparison of the simulations with the model of a cross section of muscle block in a bath (*a–d*), with the experimental results of Spach et al. (*e–h*). *e*, *f*, and *h* are redrawn from part of the paper by Spach et al. (1987), and *g* is redrawn from part of figure 2 of the paper by Spach and Kootsey (1983). dV_i/dt, Rate of change of the intracellular potential, V_i. V_e, Extracellular potential. LP, TP, Longitudinal and transverse propagation. In *a–d*, for TP, R_i = 9.0 kΩ cm, and for LP, R_i = 0.18 kΩ cm.

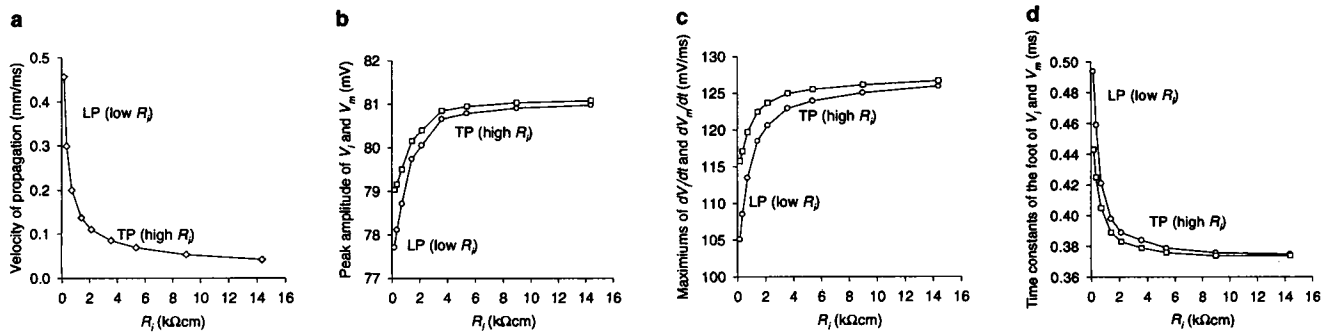

FIGURE 4 The simulation of anisotropic propagation. The effect of varying the intracellular resistivity, R_i, on the propagation velocity, the peak amplitudes (V_i^{peak} and V_m^{peak}), the maximum rate of change of membrane potential (dV_i/dt_{max} and dV_m/dt_{max}), and the time constants of the foot (τ_i and τ_m) of the intracellular and transmembrane potentials. As indicated in each figure, the low R_i and the high R_i sections of the curves correspond to the longitudinal and the transverse progagations (LP and TP). ○, Intracellular parameters; □, transmembrane parameters.

depth fibers, θ_z^{-1}, and the peak-to-peak amplitude of extracellular potential change with depth in the tissue. As shown in Fig. 5 *a*, surface fibers activated earlier than the fibers in the depth of the tissue. Near the surface, θ_z^{-1} is higher for LP than for TP, and decreases to zero as the depth is increased (in Fig. 5 *b*). Fig. 5 *c* shows that the peak to peak of extracellular potential increases with the depth in muscle. A comparison of the experimental results and the simulated results is shown in Table 1.

Simulations designed to verify the simulation model showed that the stimulation and boundary effects are limited mostly to the first and last 100 elements of the 300-element fiber, the middle section being relatively free of them. Furthermore, a change in Δx from 10 μm to 30 μm resulted in a maximum change of ~1.6%, and a change in Δt of the Crank-Nicolson PDE solver from 0.5 to 0.1 μs resulted in a maximum change of ~0.8% in the simulation results of τ_i, τ_m, V_e^{pp}, $\dot{V}_i^{max}$, and $\dot{V}_m^{max}$, showing that the choices of Δx and Δt did not introduce significant error.

DISCUSSION

The work in this paper typifies one of the most difficult problems in the theory and simulation of biological systems: achieving the optimum level of abstraction. Much more is

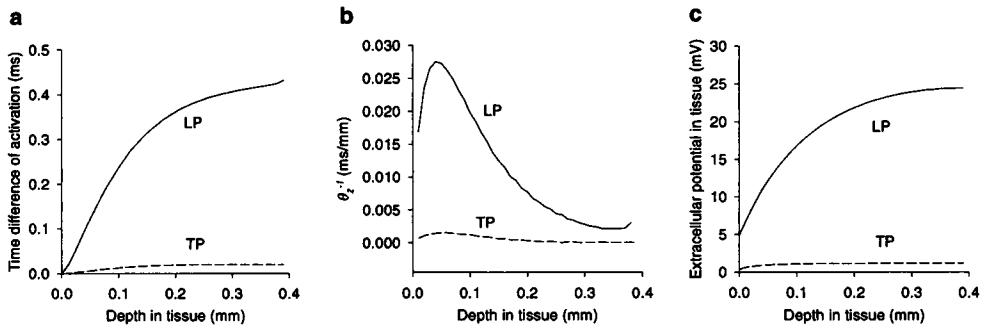

FIGURE 5 The time difference of activation, θ_z^{-1}, and extracellular potential change with the depth in muscle. (*a*) Transverse propagation (TP, dash line, R_i = 9.0 kΩ cm) has a smaller time difference of activation between surface and depth fibers than longitudinal propagation (LP, solid line, R_i = 0.18 kΩ cm). The depth zero is at the interface of bath and muscle. The time difference zero is at the middle point of the surface line in the model of a vertical cross section of a block of tissue in bath. (*b*) θ_z^{-1} is lower as the depth increases. (*c*) Extracellular potential increases as the depth in tissue increases.

known about the details of the geometry of cardiac muscle than is included in the model in this paper. If too many of these details are included, both the theory development and the computation for the simulation would become difficult or impossible. If too few details of tissue geometry are included, the calculated results do not account for the experimental observations.

The classical 1-D cable has been used for many studies of propagation in nerve and muscle cells, but this model has not been able to account for the observations of anisotropic propagation in cardiac muscle. The challenge is to find the minimum set of additions to this basic propagation model that will expand its behavior to match the observations. Previous attempts at adding details (such as discreteness) to the 1-D cable have not succeeded. In this paper we present a modest set of geometrical additions that do account for the experimental results.

The quasi-1-D theory as an extension of the classical 1-D cable theory

Compared to the classical 1-D cable (Eq. 1), the quasi-1-D cable (Eq. 22) has a coupling current, $i_i^z(x, t)$, and an additional term on the right side of the equations that relates to the extracellular potential and resistances:

$$-\frac{r_e}{r_d(r_i + r_e)} V_e(x, t).$$

The quasi-1-D cable returns to the classical cable when the coupling current, $i_i^z(x, t)$, is zero and V_e is zero, or R_d is very high, or $R_i/\gamma R_e$ is very high. This corresponds to an isolated fiber with extracellular space at isopotential ($V_e(x, t)$ is zero) and in oil (R_d is very large). In the case of an isolated fiber, when R_d is very small, both the extracellular potential $V_e(x, t)$ and its second-order derivative $\partial^2 V_e(x, t)/\partial t^2$ will be negligibly small. The $\partial^2 V_e(x, t)/\partial t^2$ term in Eq. 33 is negligible. Equation 33 can be simplified to Eq. 37:

$$V_e(x, t) = \frac{aR_d}{2\theta_x^2 R_i} \frac{\partial^2 V_m(x, t)}{\partial t^2}. \quad (37)$$

In the case of isolated fiber, $I_i^z(x, t)$ is zero. Importing Eq. 37 into Eq. 23 yields the classical 1-D cable equation (Eq. 1). The quasi-1-D cable equation reverts to the classical cable equation when it is isolated and in any of following

TABLE 1 Characteristics of simulated and experimentally recorded potentials

	Velocity (m/s)	Peak to peak of V_e (mV)	Amplitude of V_i (mV)	Maximum rate of rise of V_i (V/s)	Time constant of the foot of V_i (μs)
Experimental (dog atrium, Spach et al., 1981)					
TP	0.1	2.0	113	191	290
LP	1.0	7.0	111	144	375
TP/LP ratio	0.1	0.286	1.02	1.33	0.773
Simulated (a vertical cross section of a block of muscle in bath, R_i: 9.0 (TP), 0.18 (LP) kΩ cm)					
TP	0.0535	0.3760	80.91	125.1	376
LP	0.4566	4.0258	77.70	105.1	494
TP/LP ratio	0.117	0.0934	1.041	1.19	0.761
Simulated (1-D fiber with anisotropic membrane capacitance, Spach et al., 1987)					
TP (C_m: 0.5 μF/cm^2)			101	291	200
LP (C_m: 1.0 μF/cm^2)			92	189	280
TP/LP ratio			1.10	1.54	0.71

cases: near zero R_d, near infinite R_d, near zero V_e, near zero R_e, and near infinite R_i.

The effects of tissue resistivities

The addition of the intracellular coupling and extracellular depth currents in effect adds two new terms to the classical 1-D equations—one modifies the apparent membrane capacitance, and the other appears as an addition to the term describing the transmembrane ionic current, adding in effect a virtual membrane capacitance and a virtual membrane current, respectively. Both depend on tissue resistivities; the virtual membrane ionic current also depends on the extracellular potential, V_e, whereas the virtual membrane capacitance does not. As can be seen from Eq. 32, a higher r_i decreases V_e. So V_e is much smaller in TP compared to LP, as observed experimentally by Spach et al. (1979). With the higher anisotropic ratio of intracellular resistivity and lower anisotropic ratio of extracellular resistivity in cardiac muscle, the ratio of intracellular to extracellular resistivity is much lower in the longitudinal than in the transverse direction of the fibers. Because of the larger extracellular currents, the extracellular resistivity makes a larger contribution during LP than during TP.

Because cardiac muscle fibers are well connected to each other electrically, when steady propagation is achieved far away from the site of stimulation the wave front of propagation in a given direction will have one velocity for all fibers throughout the depth z of the muscle, with the wave front profile leading in the surface fibers and progressively lagging in the direction z for deeper fibers. As a result, the isochrone of the wave front in the z direction is curved, more so at the surface than in the depth of the muscle. There, given sufficient depth, the isochrones are close to vertical and θ_z^{-1} have low values, whereas for the surface fibers θ_z^{-1} is higher. Because of the larger contribution of extracellular resistance for LP than for TP, the curvature of the wave front near the surface of the muscle is much larger for LP than for TP. As shown in Fig. 5 *b*, near the surface of the muscle θ_z^{-1} is higher for LP than for TP. Similar wave fronts were demonstrated by Henriquez and Plonsey (1990) and Roth (1991) in their simulations of propagation along a thick strand of cardiac muscle. The higher θ_z^{-1} for LP increases the apparent membrane capacity significantly. On the other hand, for TP, because of the smaller θ_z^{-1}, the term is insignificantly small, so that the C_{app} approaches the specific membrane capacity C_m. If extracellular space is assumed to be at isopotential, as was the case in the simulations of Spach et al. (1987), the virtual membrane ionic current in Eq. 28 disappears, transforming it essentially to that of Spach et al. (1987). As pointed out previously, they could account for the anisotropies in the waveform of the AP observed experimentally, as well as the anisotropy in the safety factor for propagation when they assumed (arbitrarily) a larger specific membrane capacitance for LP than for TP. The current exchange between surface and deeper fibers, as described in the quasi-1-D theory, thereby provides a rational basis for their hypothesis of directional differences in membrane capacitance. Spach et al. were unable to account for the anisotropies in extracellular potentials, because they used 1-D cable theory with the assumption that extracellular space was at isopotential.

Although the simulations by Spach et al. (1987) used the same equations to describe Na^+ current as were used here (Ebihara and Johnson, 1980), the rate of rise of the intracellular potentials that they computed are higher than those of the present study (see Table 1 and Fig. 3). The reasons for this are twofold: Spach et al. (1987) assumed that C_m for TP was smaller (0.5 $\mu F/cm^2$) than for LP (1.0 $\mu F/cm^2$), and second, we used the measured value of 1.3 $\mu F/cm^2$ rather than the arbitrary value of 1.0 $\mu F/cm^2$.

This research was supported in part by National Institutes of Health grants RR01693, HL11307, and HL46681.

REFERENCES

Beeler, G. W., and H. Reuter. 1977. Reconstruction of the action potential of ventricular myocardial fibres. *J. Physiol. (Lond.).* 268:177–210.

Berkinblit, M. B., N. D. Vvedenskaya, I. Dudzyavichus, S. A. Kovalev, S. V. Fomin, A. V. Kholopov, and L. M. Chailakhyan. 1970. Investigation of the spread of excitation in the Purkinje fibres of the heart in a mathematical model. *Biophysics (Biofizika).* 15:545–551.

Clerc, L. 1976. Directional differences of impulse spread in trabecular muscle from mammalian heart. *J. Physiol. (Lond.).* 255:335–346.

Diaz, P. J., Y. Rudy, and R. Plonsey. 1982. A model study of the effect of intercalated discs on discontinuous propagation in cardiac muscle. *Adv. Exp. Med. Biol.* 161:79–89.

Dominguez, G., and H. A. Fozzard. 1979. Effect of stretch on conduction velocity and cable properties of cardiac Purkinje fibers. *Am. J. Physiol.* 237:C1190–C124.

Ebihara, L., and E. A. Johnson. 1980. Fast sodium current in cardiac muscle—a quantitative description. *Biophys. J.* 32:779–790.

Henriquez, C. S., and Papazoglou, A. A. 1993. Conduction in a 3D bidomain representation of cardiac tissue with unequal anisotropy. *In* Proceedings of the 15th Annual International Conference of the IEEE Engineering in Medicine and Biology Society, Oct. 28–31, 1993. 15(2): 748–749.

Henriquez, C. S., and R. Plonsey. 1990. Simulation of propagation along a cylindrical bundle of cardiac tissue. II. results of simulation. *IEEE Trans. Biomed. Eng.* 37:861–875.

Hodgkin, A. L., and A. F. Huxley. 1952. A quantitative description of membrane current and its application to conduction and excitation in nerve. *J. Physiol. (Lond.).* 117:500–544.

Hodgkin, A. L., and B. Katz. 1949. The effect of sodium ions on the electrical activity of the giant axon of the squid. *J. Physiol. (Lond.).* 108:37–77.

Hodgkin, A. L., and W. A. H. Rushton. 1946. The electrical constants of a crustacean nerve fibre. *Proc. R. Soc. Ser. B.* 133:444–479.

Hoyt, R. H., M. L. Cohen, and J. E. Saffitz. 1989. Distribution and three-dimensional structure of intercellular junctions in canine myocardium. *Circ. Res.* 64:563–574.

Johnson, E. A., and J. R. Sommer. 1967. A strand of cardiac muscle: its ultrastructure and the electrophysiological implication of its geometry. *J. Cell Biol.* 33:103–129.

Joyner, R. W. 1982. Effects of the discrete pattern of electrical coupling on propagation through an electrical syncytium. *Circ. Res.* 50:192–200.

Joyner, R. W., F. Ramon, and J. W. Moore. 1981. Simulation of action potential propagation in an inhomogeneous sheet of coupled excitable cells. *Circ. Res.* 36:654–661.

Kootsey, J. M., and J. Wu. 1991. Models of electrophysiological activation. *In* Imaging, Measurement and Analysis of the Heart. S. Sideman and R. Beyar, editors. Hemisphere Publishing Corporation, New York. 373–381.

Kukushkin, N. I., F. F. Bukauskas, M. Ye. Sakson, and V. V. Nasonova. 1975. Anisotropy of steady speeds and delays of the extrasystolic waves in the heart of the dog. *Biophysics (Biofizika).* 20:687–692.

Leon, L. J., and F. A. Roberge. 1991. Structure complexity effects on transverse propagation in a two-dimensional model of myocardium. *IEEE Trans. Biomed. Eng.* 38:997–1009.

Lieberman, M., T. Swanobori, J. M. Kootsey, and E. A. Johnson. 1975. A synthetic strand of cardiac muscle: its passive electrical properties. *J. Gen. Physiol.* 65:527–550.

Mathias, R. T., L. Ebihara, M. Lieberman, and E. A. Johnson. 1981. Linear electrical properties of passive and active currents in spherical heart cell clusters. *Biophys. J.* 36:221–242.

Plonsey, R. 1974. The active fiber in a volume conductor. *IEEE Trans. Biomed. Eng.* BME-21:371–381.

Plonsey, R., and R. C. Barr. 1988. Bioelectricity. Plenum Press, New York.

Pollard, A. E., N. Hooke, and C. S. Henriquez. 1992. Cardiac propagation simulation. *Crit. Rev. Biomed. Eng.* 20:171–210.

Roberts, D., L. T. Hersh, and A. M. Scher. 1979. Influence of cardiac fiber orientation on wavefront voltage, conduction velocity, and tissue resistivity in the dog. *Circ. Res.* 44:701–712.

Roth, B. J. 1991. Action potential propagation in a thick strand of cardiac muscle. *Circ. Res.* 68:162–173.

Rudy, Y., and W. Quan. 1987. A model study of the effects of the discrete cellular structure on electrical propagation in cardiac tissue. *Circ. Res.* 61:815–823.

Shiba, H. 1971. Heaviside's "Bessel cable" as an electric model for flat simple epithelial cells with low resistive junctional membranes. *J. Theor. Biol.* 30:59–68.

Shiba, H., and Y. Kanno. 1971. Further study of the two-dimensional cable theory: an electric model for a flat thin association of cells with a directional intercellular communication. *Biophysik.* 7:295–301.

Shibata, N., P. S. Chen, E. G. Dixon, P. D. Wolf, N. D. Danieley, W. M. Smith, and R. E. Ideker. 1988. Influence of shock strength and timing on induction of ventricular arrhythmias in dogs. *Am. J. Physiol.* 255: H891–H901.

Sommer, J. R., and E. A. Johnson. 1979. Ultrastructure of cardiac muscle. *In* R. M. Berne, N. Sperelakis, and S. R. Geiger, editors. Handbook of Physiology, The Cardiovascular System I. American Physiological Society, Bethesda, MD. 113–186.

Sommer, J. R., and B. Scherer. 1985. Geometry of cell and bundle appositions in cardiac muscle: light microscopy. *Am. J. Physiol.* 248: H792–H803.

Spach, M. S. 1983. The discontinuous nature of electrical propagation in cardiac muscle. *Ann. Biomed. Eng.* 11:209–261.

Spach, M. S., P. C. Dolber, J. F. Heidlage, J. M. Kootsey, and E. A. Johnson. 1987. Propagating depolarization in anisotropic human and canine cardiac muscle: apparent directional differences in membrane capacitance. A simplified model for selective directional effects of modifying the sodium conductance on $\dot{V}_{max}$, τ_{foot}, and the propagation safety factor. *Circ. Res.* 60:206–219.

Spach, M. S., J. F. Heidlage, E. R. Darken, E. Hofer, K. H. Raines, and C. F. Starmer. 1992. Cellular reflects both membrane properties and the load presented by adjoining cells. *Am. J. Physiol* 263 *(Heart Circ. Physiol.* 32): H1855–H1863.

Spach, M. S., and J. M. Kootsey. 1983. The nature of electrical propagation in cardiac muscle. *Am. J. Physiol.* 244:H3–H22.

Spach, M. S., W. T. Miller, D. B. Geselowitz, R. C. Barr, J. M. Kootsey, and E. A. Johnson. 1981. The discontinuous nature of propagation in normal canine cardiac muscle. Evidence for recurrent discontinuities of intracellular resistance that affect the membrane currents. *Circ. Res.* 48:39–54.

Spach, M. S., W. T. Miller, E. Miller-Jones, R. B. Warren, and R. C. Barr. 1979. Extracellular potentials related to intracellular APs during impulse conduction in anisotropic canine cardiac muscle. *Circ. Res.* 45:188–204.

Tung, L. 1978. A bidomain model for describing ischemic myocardial D.C. potentials. Ph.D. dissertation. MIT, Cambridge, MA.